Operating characteristics and comparison of photopyroelectric and piezoelectric sensors for trace hydrogen gas detection. I. Development of a new photopyroelectric sensor

Constantinos Christofides and Andreas Mandelis
Photoacoustic and Photothermal Sciences Laboratory, Department of Mechanical Engineering, and Center for Hydrogen and Electrochemical Studies (CHES), University of Toronto, Toronto, Ontario M5S 1A4, Canada

(Received 7 February 1989; accepted for publication 11 July 1989)

A new type of solid-state sensor for the detection of minute concentrations of hydrogen gas has been developed. The sensor was made of thin, commercially available polyvinylidene fluoride (PVDF) pyroelectric film, sputter coated with Pd. An infrared laser beam served to produce alternating temperature gradients on the Pd-PVDF and on reference Al-Ni-PVDF films, which, in turn, generated ac voltages due to the photopyroelectric (P^2E) effect. Exposure to hydrogen gas was shown to produce an increased differential signal between the Pd and reference electrodes; this was tentatively attributed to the adsorption and dissociation of hydrogen molecules on the Pd surface, which caused a shift on the Pd-PVDF pyroelectric coefficient, due to interactions at the Pd-PVDF interface. The differential signal was found to be proportional to the square root of the hydrogen partial pressure at very low concentrations (< 1000 ppm). A semiquantitative interpretation of the differential signal has been achieved using simple gas-solid interaction theory and the combination of the Langmuir isotherm with the photopyroelectric theory in the range of 4–200 Pa. For high pressures (> 200 Pa) the paper is limited only to a phenomenological description. The thickness of the palladium layer has been found to play an important role with respect to the signal response. Presently, hydrogen concentrations as small as 40 ppm, in a flowing $H_2 + N_2$ mixture, have been detected. The influence of gas flow rate has also been studied. Other characteristics such as the response times, the reversibility, and the durability of the Pd-PVDF-P^2E hydrogen detector will also be presented.

I. INTRODUCTION

We will deal with two different hydrogen sensors based on catalytic palladium in this and the following paper. In this paper we will describe and analyze a new photopyroelectric (P^2E) solid-state sensor. The second paper (part II)[1] contains an analysis of a piezoelectric sensor for hydrogen, used for comparison with the P^2E device performance under gas flow-through conditions.

In recent years, a considerable research effort has been directed toward the development of hydrogen gas sensors. As of 1966, a number of gas sensors based on hydrogen-induced changes in the electrical conductivity of metal-oxide-semiconductor (MOS) structures have been reported.[2–4] Furthermore, Lundström, Shivaraman, and Svensson developed a Pd-gate MOS transistor and Pd-gate metal-insulator-semiconductor (MIS) sensors,[5,6] while Steele and MacIver showed that a Pd-CdS Schottky barrier diode exhibited a response to hydrogen.[7] The double metal-gate MIS field-effect transistor (FET) has also been used as a hydrogen sensor,[8] and so has been the insulated-gate field-effect transistor (IGFET),[5,9] as well as the hydrogen-sensitive MOSFETs with a catalytic gate metal, such as Pd.[5] A variety of other hydrogen sensors have also been developed: a surface acoustic wave (SAW) sensor,[10] an optical fiber sensor,[11] a hydrogen uranyl phosphate (HUP) detector,[12,13] and a piezoelectric crystal detector.[1,14] There exist also in the market several non-solid-state sensors for hydrogen, such as the flame ionization detector (FID)[15] which is often used. A pyroelectric gas sensor, based on dc surface temperature changes due to heats of adsorption and desorption following thermal ramping of the sensor, has also been reported.[16] This sensor requires a furnace-type environment for temperature ramping, and its sensitivity to trace gas analysis under dynamic, flow-through conditions has not been established. Severe noise problems due to surface temperature transients under flow conditions might be expected to limit the utility of this sensor. Zemel[17] has recently fabricated a $LiTaO_3$ pyroelectric detector based on gas-surface interaction principles, which requires multilevel planar processing and is activated by resistive dc heating via a thin-film (400-nm) NiCr heater. Besides its fabrication complexity, this dc pyroelectric sensor has proven to be extremely susceptible to temperature fluctuations due to environmental factors (e.g., valve opening and closing during gas flow cycles). An additional disadvantage of this (otherwise quite sensitive) sensor may be the long delay for gas detection due to diffusive transport of thermal energy from the Pd electrode region to the reference (Au) electrode. These factors appear to have limited the development of purely pyroelectric devices as gas sensors to date.

This paper describes the development of a novel, fast, and simple thin-film photopyroelectric (P^2E)[18–20] solid-state sensor for the detection of minute concentrations of

 0021-8979/89/213975-11$02.40

hydrogen gas, with distinct advantages over other sensors under STP conditions. The present P^2E device is expected to solve many problems encountered with purely pyroelectric, and perhaps other, gas detectors, with the added element of fabrication simplicity. The experimental characteristics of the Pd-PVDF-P^2E sensor under gas flow-through conditions will be compared to those of the well-established piezoelectric sensor in the accompanying paper.

II. PHOTOPYROELECTRIC SIGNAL GENERATION

The phenomenon of pyroelectricity is not new. It was observed almost 300 years ago. Several theoretical and experimental studies of the pyroelectric effect have been performed during the last 20 years. Pyroelectricity is the manifestation of the spontaneous polarization dependence of certain anisotropic solids on temperature. This effect is exhibited only by solids which satisfy crystallographic requirements such as (i) the crystal lattice must have no center of symmetry and (ii) the crystal must have no more than one axis of rotational symmetry. A pyroelectric material becomes electrically neutral when in a constant temperature environment for a period of time. If there is a small change of the temperature, ΔT, the pyroelectric material becomes electrically polarized and a voltage arises between certain directions in the material. This unique property of pyroelectric materials led to many applications during the last few years. The pyroelectric thermometer,[21,22] the pyroelectric anemometers,[23] the dc pyroelectric gas sensor,[17] and the radiation monitor[24] may be counted among others.

Pyroelectricity also arises in certain noncentrosymmetric quasiamorphous polymers such as polyvinylidene fluoride (PVDF). In these materials the change of polarization causes a current rise external to the polymer. The output measured voltage under load conditions may be written as[17]

$$V(t)=\frac{PA\exp(-t/\tau)}{C}\int_0^t \exp\left(\frac{t'}{\tau}\right)\left(\frac{dT}{dt'}\right)dt', \qquad (1)$$

where P is the pyroelectric coefficient, A is the total pyroelectric film area, t is the time, $C=C_p+C_A$ with C_p being the pyroelectric capacitance and C_A the input capacitance of the amplifier, and τ is a characteristic electronic time constant ($\tau=RC$; $R=[(1/R_p)+(1/R_A)]^{-1}$ where R_p and R_A are the resistance of the pyroelectric capacitor and of the preamplifier input, respectively). $\langle T\rangle$ is the instantaneous temperature rise of the pyroelectric averaged over its thickness. If the temperature varies harmonically as a function of optical irradiance modulation frequency f, the photopyroelectric voltage will be

$$V(f)=\frac{2\pi j fPRA\langle T\rangle}{1+2\pi j f\tau}. \qquad (2)$$

The temperature distribution across the pyroelectric film (z direction) may be estimated using the Fourier heat-conduction equation:

$$\frac{\partial T}{\partial t}=D_T\frac{\partial^2 T}{\partial z^2}, \qquad (3)$$

where D_T is the thermal diffusivity of the pyroelectric film, defined as the ratio of the thermal conductivity k to the volume heat capacity C_v. Thus it is easy to show that

$$\left\langle\frac{\partial T}{\partial t}\right\rangle=\frac{k}{C_v}\left\langle\frac{\partial^2 T}{\partial^2 z}\right\rangle=\frac{1}{C_v z_0}\Delta H(t), \qquad (4)$$

where $\Delta H(t)=H(0,t)-H(z_0,t)$ is the net heat flux into the pyroelectric film of thickness z_0. Substituting Eq. (4) into Eq. (1) leads to

$$V(t)=\frac{PA\exp(-t/\tau)}{CC_v z_0}\int_0^t \Delta H(t')\exp\left(\frac{t'}{\tau}\right)dt'. \qquad (5)$$

Considering that the pyroelectric response at $t=\tau_{\rm th}$ ($\tau_{\rm th}$ is the thermal time constant) is long compared to the RC time constant τ of the film (typical values of τ are of the order of 10 ms; 5 ms in this work; see Tables I and II), Eq. (5) may be simplified in the form[17]

$$V(t)=\frac{PRA}{C_v z_0}\Delta H(t). \qquad (6)$$

In our frequency domain experiments, using laser-beam intensity-modulation frequencies f less than 20 Hz, the condition $\tau\ll\tau_{\rm th}$ was always satisified in the form $2\pi f\tau\ll 1$, and Eq. (6) will thus be used in all subsequent discussion with $t\to f$. The same result may be obtained directly using Eq. (2) with the above condition.

TABLE I. Some experimental parameters using for P^2E measurements.[a]

Experimental parameters	
Pyroelectric film thickness, z_0 (cm)	2.8×10^{-3}
Amplifier input resistance at 20 Hz, R_A (Ω)	10^8
Amplifier input capacitance, C_A (pF)	16
Pd thickness, L (cm)	2.85×10^{-6}
Pd total area, A (cm^{-2})	0.1

[a] From Ref. 25.

III. EXPERIMENTAL APPARATUS

A. Pd-PVDF sensor design

Poled PVDF thin films (β phase) are known to exhibit strong pyroelectricity; i.e., a potential difference is generated in the direction of poling between the two metallized electrode surfaces which sandwich the pyroelectric film when a temperature change is induced within the pyroelectric layer.[25] The design of a hydrogen sensor fabricated from such a

TABLE II. Some properties of PVDF pyroelectric film.[a]

Properties of PVDF	
Dielectric permittivity, ϵ (F/cm)	1.06×10^{-12}
Relative permittivity, ϵ/ϵ_0	12
Capacitance, C_p (pF)	37.9
Pyroelectric coefficient (at 20 °C), p_e (C/cm^2 K)	3×10^{-9}
Volume resistivity (Ω cm)	1.5×10^{15}
Density (g/cm^3)	1.78
Thermal diffusivity D_T, (cm^2/s)	5.2×10^{-4}
Thermal time constant $\tau_{\rm th}$ (s)	5

[a] From Ref. 25.

pyroelectric thin film has become feasible owing to the possibility of depositing a variety of thin metal electrode coatings on PVDF. In this work, PVDF was coated with Pd metal which can adsorb and subsequently absorb hydrogen gas molecules preferentially in the presence of other ambient gases. Our hypothesis was that, upon establishing an ac steady-state temperature field within the pyroelectric by amplitude-modulated laser irradiation, any changes in the temperature distribution and/or the pyroelectric coefficient of the PVDF, due to interactions with the hydrogen gas, would be registered as changes in the observed P^2E signal, thus yielding a hydrogen sensor.

It is well known that both palladium (Pd) and nickel (Ni) have high hydrogen solubilities. At room temperature the H_2 is more than a 1000 times more soluble in Pd than in Ni.[26] Because of its selectivity to hydrogen absorption, palladium has been preferred as a filter for hydrogen purification[26] and has also been used to provide hydrogen selectivity for piezoelectric hydrogen detectors.[1,14] The Pd-PVDF film was placed in a standard Inficon housing as described elsewhere.[27]

B. Gas mixing system

A system has been constructed which has allowed testing the response of the Pd-PVDF-P^2E sensor to flows of hydrogen/nitrogen mixtures, with H_2 concentrations ranging from 10 ppm to pure hydrogen (Canadian Liquid Air: ultra high purity 99.999%). The system consisted of three subsystems: gas control, temperature control, and test cell [see Fig. 1(a)].

The gas control system mixed the nitrogen and hydrogen gases in a homogeneous flow. The flow rate of each gas could be adjusted and stabilized before the mixture was directed into the test cell. The system included tanks of nitrogen and hydrogen gas, pressure regulators, flow meters, valves, a pump, and the manifold lines which interconnected all of these components. Figure 1(a) shows the complete experimental setup. The gas handling system introduced a mixture of hydrogen and nitrogen gases into the test cell and allowed the mixture to leave through the exhaust line after pumping.

The temperature control system ensured that the temperature of the incoming gas flow would be the same as that of the sensor itself. A heat-exchange coil was installed on the gas mixture line, upstream from the test cell. The test cell and heat-exchange coil were suspended in a water bath to equalize their temperatures. A thermocouple allowed the monitoring of the cell temperature during the experiments. Past the heat exchanger, the gases passed through a three-way valve. This valve was able to direct the gases either into the test cell or into the bypass line and then to the exhaust [Fig. 1(a)]. In this way, flow could be established and stabilized before it was introduced into the test cell.

The test cell was the heart of the experimental system,

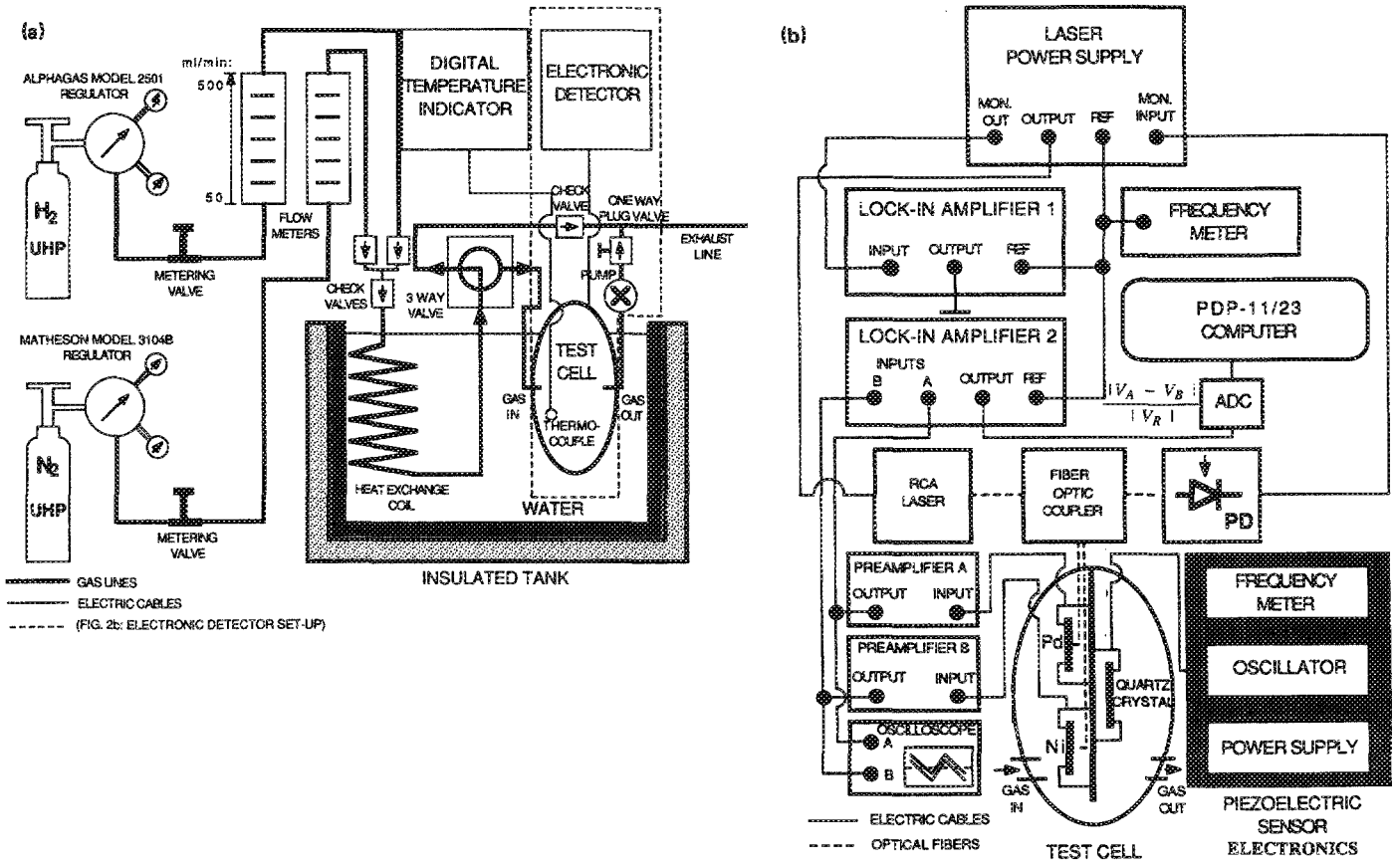

FIG. 1. (a) Schematic diagram of the experimental system. (b) Schematic diagram of the photopyroelectric and piezoelectric detector setup.

containing two P^2E detectors (active Pd coated and reference Ni-Al coated) and one control Pd-coated piezoelectric quartz-crystal microbalance detector. It consisted of a pressure vessel, which contained the P^2E and the piezoelectric quartz-crystal detectors. The principle of operation of a single piezoelectric sensor has been described previously.[14] The experimental setup of the control piezoelectric quartz-crystal detector is shown schematically at the lower center of Fig. 1(b). The piezoelectric instrumentation is described in part II.[1]

C. P^2E signal generation and detection

The signal generation and analysis setup of the P^2E sensor is described in Fig. 1(b). The instrumentation consisted of an RCA laser diode (model C86006E GaAlAs infrared laser diode, manufactured by RCA New Products Division) powered by an ac current supply (maximum output current: 70 mA). The output laser beam, 4 mW *p-t-p* multimode at ca. 800 nm, was directed to a CANSTAR three-way model fiber-optic coupler where it was split at approximately 16%, 34%, and 50%. The 16% intensity fiber-optic channel was directed to a photodiode (PD) whose output was then sent to the "monitor" input of the homemade laser current supply for preamplification and feedback control of the laser current, as well as for synchronous lock-in detection. The feedback control consisted of using this reference signal to correct for temporal intensity variations in the modulated laser beam. The modulation frequency of the infrared beam was monitored with a frequency meter. It is important to note that the optical absorptance of the metallized PVDF film in the infrared region of the spectrum is very high (80%–95%)[25] so that sensor operation was in the photopyroelectric saturation regime,[28] independent of the optical properties of the coated PVDF. The ac P^2E detector signals from a 28-μm-thick PVDF film, on which a thickness of Pd $\sim$285 Å has been coated (henceforth designated "unit A"), and a similar PVDF film covered with standard 200 Å of Pennwalt Ni and then with 600 Å of Al ("unit B"), were bandpass filtered and preamplified by two low-noise Ithaco preamplifiers (model 1201). The two signals were then connected to a double-input Tektronix (model T912) oscilloscope for visual display and to two lock-in analyzers (EG&G model 5204), designated units 1 and 2 [see Fig. 1(b)]. The lock-in amplifiers were referenced by the ac laser current supply. The output of lock-in 1 was connected to lock-in amplifier 2, which was equipped with a ratio option, allowing a normalized function output:

$$\Delta S = \frac{|V_A - V_B|}{|V_R|}, \tag{7}$$

where V_A is the signal obtained by the Pd-PVDF electrode, V_B is the signal generated by the Al-Ni-PVDF electrode, and V_R is the ac laser power reference output obtained from the photodiode PD. From Eq. (6) the normalized output signal obtained by the Pd-PVDF, S_{Pd}, and the Al-Ni-PVDF, $S_{\mathrm{Ni\text{-}Al}}$, electrodes may be written as[19,20]

$$S_{\mathrm{Pd}}(f) \equiv \frac{V_A}{|V_R|} = \frac{1}{|V_R|}\frac{AR}{z_0 C_v}\Delta H_{\mathrm{Pd}}(f) P_{\mathrm{Pd}}, \tag{8a}$$

$$S_{\mathrm{Ni\text{-}Al}}(f) \equiv \frac{V_B}{|V_R|} = \frac{1}{|V_R|}\frac{AR}{z_0 C_v}\Delta H_{\mathrm{Ni\text{-}Al}}(f) P_{\mathrm{Ni\text{-}Al}}, \tag{8b}$$

where ΔH_{Pd} and $\Delta H_{\mathrm{Ni\text{-}Al}}$ are the net heat fluxes into the Pd-PVDF and Al-Ni-PVDF P^2E devices, repectively; P_{Pd} and $P_{\mathrm{Ni\text{-}Al}}$ are the pyroelectric coefficients of the Pd- and Al-Ni-coated PVDF films, respectively; and f is the laser-diode current-modulation frequency. The lock-in output channels were connected to a PDP-11/23 computer, through the ports of an A/D converter, for data storage and analysis of the ratioed output signal amplitude ΔS.

As was described above, two output infrared beams were directed to the Pd-PVDF and Al-Ni-PVDF films. The two pyroelectric transducers absorbed the thermal energy of the infrared beams and thus gave rise to two different electrical voltages V_A and V_B. In our case, harmonic modulation of the beam intensity resulted in harmonic changes in ΔT, which subsequently gave rise to synchronous ac voltages V_A and V_B. From Eqs. (7), (8a), and (8b), the differential normalized output signal may be written as[19,20]

$$\Delta S(f) = |S_{\mathrm{Pd}}(f) - S_{\mathrm{Ni\text{-}Al}}(f)| = \frac{1}{|V_R|}\frac{AR}{z_0 C_v}|\Delta H_{\mathrm{Pd}}(f) P_{\mathrm{Pd}} - \Delta H_{\mathrm{Ni\text{-}Al}}(f) P_{\mathrm{Ni\text{-}Al}}|. \tag{9}$$

Since the heat flows into the P^2E devices from the laser beams were not very different, the differential voltage was very small under equal preamplifier gains. The magnitude of ΔS was further minimized ($\Delta S \approx 0$) at the beginning of each experiment by a judicious choice of gain on the preamplifiers, before the introduction of the gas into the test cell. In fact, according to Eq. (9), the minimizing of $\Delta S(\Delta S \to 0)$ led to

$$\Delta H_{\mathrm{Pd}} P_{\mathrm{Pd}} \approx \Delta H_{\mathrm{Ni\text{-}Al}} P_{\mathrm{Ni\text{-}Al}}. \tag{10}$$

Thus, before the introduction of H_2 into the test cell, the difference between the net heat fluxes ΔH_{Pd} and $\Delta H_{\mathrm{Ni\text{-}Al}}$ was eliminated because of the choice of the preamplifier gains. On the other hand, in the absence of H_2 gas ($[\mathrm{H}] = 0$), the pyroelectric coefficients of the Pd- and Ni-Al-coated PVDF films may be assumed identical: $P_{\mathrm{Pd}}[0] = P_{\mathrm{Ni\text{-}Al}}[0]$. As a result of the above consideration, we can write that $\Delta H_{\mathrm{Pd}} = \Delta H_{\mathrm{Ni\text{-}Al}} \equiv \Delta H$. This is taken into account for the following discussion. The introduction of hydrogen into the test cell does not change the heat fluxes because $\Delta T(f)$ is solely determined by the infrared laser beams. On the other hand, adsorption and absorption of H_2 atoms by the Pd may be expected to change the two pyroelectric coefficients P_{Pd} and $P_{\mathrm{Ni\text{-}Al}}$ which depend on the introduced hydrogen concentrations. Thus, for interaction of H_2 gas with Pd to cause an excess differential voltage δS, according to Eq. (9), we have[19,20]

$$\delta S(f) = \frac{1}{|V_R|}\frac{AR}{z_0 C_v}\Delta H(f)(P_{\mathrm{Pd}}[\mathrm{H}] - P_{\mathrm{Ni\text{-}Al}}[\mathrm{H}]). \tag{11}$$

However, $P_{\mathrm{Ni\text{-}Al}}[\mathrm{H}] = P_{\mathrm{Ni\text{-}Al}}[0] \approx P_{\mathrm{Pd}}[0]$, and this is due to the isolation of the Ni surface from the H_2 gas. This shows that in the absence of hydrogen gas, $\delta S = 0$. With the above

considerations Eq. (11) may be modified as

$$\delta S(f) = Q\Delta H(f)(P_{\mathrm{Pd}}[\mathrm{H}] - P_{\mathrm{Pd}}[0]), \qquad (12a)$$

where $Q \equiv (1/|V_R|)(AR/z_0 C_v)$ is a system constants. By writing $\Delta P_{\mathrm{Pd}} \equiv P_{\mathrm{Pd}}[\mathrm{H}] - P_{\mathrm{Pd}}[0]$, Eq. (12a) can be rewritten as

$$\delta S(f) = Q\Delta H(f)\Delta P_{\mathrm{Pd}}. \qquad (12b)$$

For small departures from the $P_{\mathrm{Pd}}[0]$ value, the density of adsorbed molecules (or atoms), N_{H}, is related to the ΔP_{Pd} variation through the derivative of the pyroelectric coefficient:

$$\Delta P_{\mathrm{Pd}} = \left(\frac{\partial P_{\mathrm{Pd}}}{\partial N_{\mathrm{H}}}\right)_{N_{\mathrm{H}}=0} N_{\mathrm{H}}. \qquad (13)$$

Using Eqs. (12b) and (13), we may finally write

$$\delta S_s(N_{\mathrm{H}}; f) = Q\left(\frac{\partial P_{\mathrm{Pd}}}{\partial N_{\mathrm{H}}}\right)_{N_{\mathrm{H}}=0} \Delta H(f) N_{\mathrm{H}_s}, \qquad (14)$$

where N_{H_s} is the saturated number of the adsorbed and absorbed hydrogen atoms, and δS_s is the differential P^2E signal in the saturation regime.

IV. RESULTS AND DISCUSSION

A. Experimental data

All of the present measurements have been performed under ambient temperature (20 °C) and background pressure (1 atm). Typical experimental results are shown in Figs. 2(a)–2(c) for various hydrogen concentrations using Pd film 285 Å in thickness. These figures show details of P^2E response as a function of time under the same temperature and flow rate conditions. We plotted the variation of δS as a function of time for hydrogen concentrations ranging from 100% to 0.075%. The concentration in this range corresponds to a hydrogen partial pressure range between 10^5 and 75 Pa. The relationship between gas concentration and Pd-PVDF-P^2E detector response at saturation $\delta S(\delta S_s)$ is an important parameter for sensor characterization. Figure 3(a) shows the variation of δS_s as a function of hydrogen concentration using data from Figs. 2(a)–2(c). Figure 3(b) shows the variation of δS_s as a function of hydrogen concentration using Pd film of 130 Å in thickness. It is important to realize that δS_s decreases very fast at low hydrogen concentrations ($[\mathrm{H}_2] < 10\%$). Between 10% and 50%, δS_s remains almost constant as a function of concentration, and it increases again for concentrations higher than 50%.

B. Surface and interface adsorption

In order to discuss the variation of Pd-PVDF-P^2E response as a function of concentration (or hydrogen partial pressure p_{H_2}), it is necessary to recall the surface-gas interaction in the hydrogen-palladium system. In this subsection we will discuss some of the parameters which determine the amount of H_2 at the palladium surface and the Pd-PVDF interface. The adsorbed hydrogen gas molecules are dissociated on the catalytic metal surface (Pd in our case), and the H atoms are absorbed into the Pd bulk. Some of these absorbed atoms diffuse to the Pd-PVDF interface. According to Lundström,[29] there is an equilibrium between the number

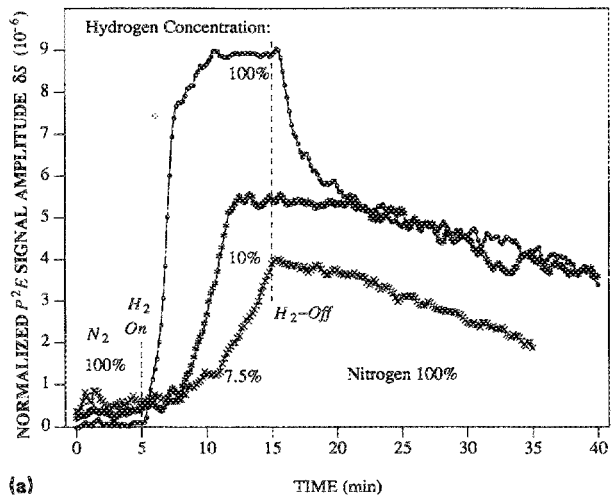

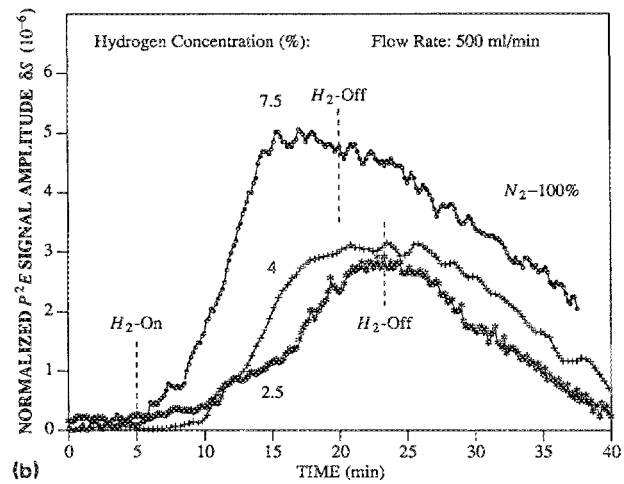

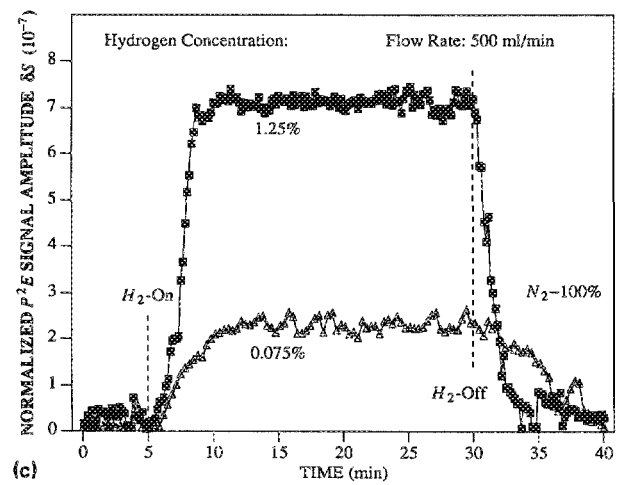

FIG. 2. Photopyroelectric response as a function of time, for various concentrations (Pd thickness = 285 Å): (a) 7.5%–100% hydrogen, (b) 2.5%–7.5% hydrogen, and (c) 1.25% and 0.075% hydrogen. Flow rates: 500 mℓ/min (T = 20 °C).

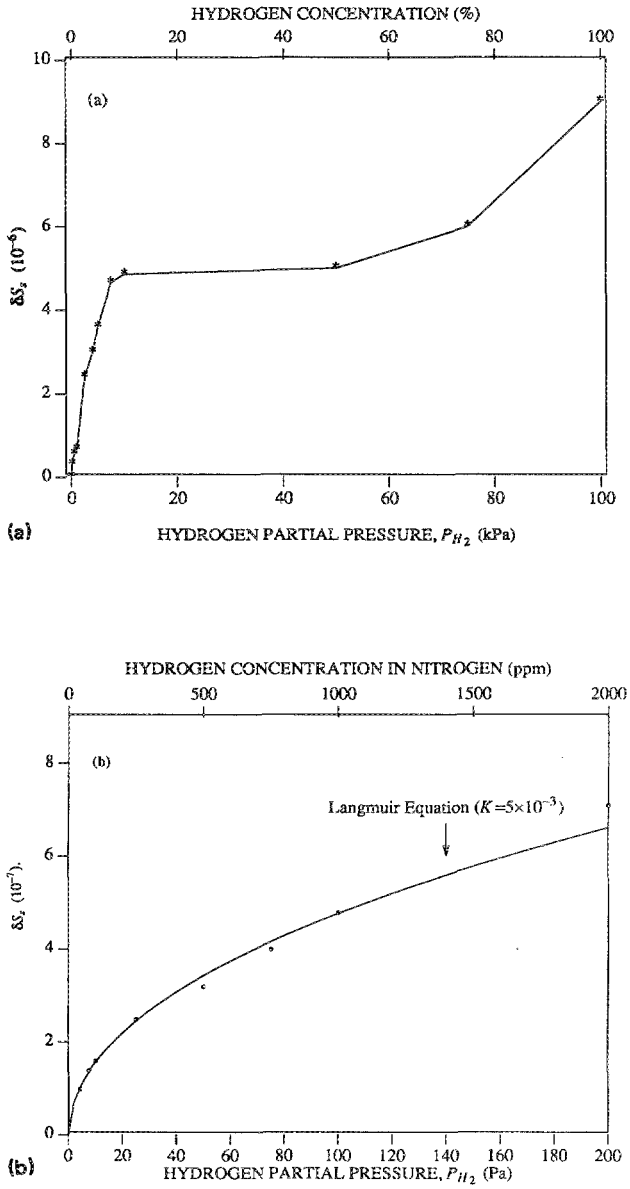

FIG. 3. Variation of output differential signal δS_s as a function of partial hydrogen pressure (or concentration). (a) Data collected from Figs. 2(a)–2(c) (Pd thickness = 285 Å). (b) Pd thickness = 130 Å. The solid curve is the fitted Langmuir isotherm [Eq. (23)].

of adsorbed H on the surface and that at the back interface. In an inert atmosphere (such as nitrogen) this H adsorbed-absorbed number depends mainly on the hydrogen pressure. Hydrogen atoms adsorbed at the surface and absorbed in the PD film are hypothesized to give rise to a differential P^2E signal upon arrival on the Pd-PVDF interface, followed by interactions with the pyroelectric dipole system of the bulk PVDF. The present situation is, phenomenologically and geometrically, similar to the back Pd-transistor gate interface detection of the MOS-hydrogen sensor.[29] Therefore, Lundström's analysis may construe a useful guide for the phenomenological interpretation of the present results, assuming similar hydrogen adsorption on, and absorption kinetics in, palladium. In the case of an inert atmosphere, the only reaction which takes place on the metal surface is[29–31]

$$\mathrm{H_2} \underset{d_1}{\overset{c_1}{\leftrightarrows}} 2\mathrm{H}_a. \tag{15a}$$

This reaction represents the dissociation of hydrogen on the Pd catalyst. H_a is the adsorbed hydrogen atom, and c_1 and d_1 are the rate constants of the reaction. After the absorption of hydrogen into, and diffusion through, the Pd film, another reaction takes place:[29,30]

$$\mathrm{H}_a \underset{c_e}{\overset{d_e}{\rightleftarrows}} \mathrm{H}_b \underset{c_i}{\overset{d_i}{\rightleftarrows}} \mathrm{H}_{ai}, \tag{15b}$$

where H_a and H_{ai} are the atomic hydrogen concentration in the bulk and at the back interface, respectively. Assuming that the number of hydrogen adsorption sites per unit area on the Pd surface is N_e, and on the Pd-PVDF interface is N_i, then one can write[30]

$$\frac{n_i}{N_i - n_i} = \frac{d_i}{c_i}\frac{n_b}{N_b - n_b} = \frac{c_e d_i}{d_e c_i}\frac{n_e}{N_e - n_e}, \tag{16}$$

where N_b is the number of absorption sites in the bulk (per unit volume$\times$thickness) of the Pd film. n_i, n_b, and n_e are the concentrations of the adsorbed hydrogen atoms on the Pd-PVDF interface, bulk, and surface. At equilibrium the forward and backward rates are equal so that[32]

$$c_1[\mathrm{H_2}] = d_1[\mathrm{H}_a]^2. \tag{17}$$

Furthermore, from Eqs. (15a) and (17),[29,30]

$$\frac{n_e}{N_e - n_e} = \sqrt{\frac{c_1}{d_1}P_{\mathrm{H_2}}}. \tag{18}$$

One can note that in Eq. (18) the partial hydrogen pressure $P_{\mathrm{H_2}}$ has been introduced, a fact which leads to a simpler interpretation of our experimental results which are basically expressed as a function of hydrogen partial pressure. Thus it is necessary to introduce the *coverage* of hydrogen at the surface, $\Theta_e = n_e/N_e$, and at the Pd-PVDF interface, $\Theta_i = n_i/N_i$. By combining the Eqs. (16) and (18) one can write[29,30,32]

$$\frac{\Theta_i}{1-\Theta_i} = A\frac{\Theta_e}{1-\Theta_e} = K\sqrt{P_{\mathrm{H_2}}}, \tag{19}$$

where $A \equiv c_e d_i / d_e c_i$, and K is a constant which depends mainly on the difference in adsorption energies at the surface and interface, respectively. According to Lundström,[29] we can assume a linear relationship between the measured response signal and the coverage of hydrogen atoms, Θ_i:

$$\delta S = \delta S_{\max}\Theta_i, \tag{20a}$$

assuming $\Theta_i = \Theta_{is}$ at the saturation regime (i.e., $t \to \infty$), Eq. (20a) may be written

$$\delta S_s = \delta S_{\max}\Theta_{is}, \tag{20b}$$

where $\delta S_{\max}$ is the maximum saturation signal response of the P^2E detector corresponding to complete (saturated) surface coverage.

C. Langmuirian analysis in low concentration regime (<2000 ppm)

In the following discussion the bulk effect will be neglected (in fact some experimental results at very high pres-

sures have shown that the P^2E response is independent of the Pd thickness). In the light of results presented by Lundström, Armgarth, and Petersson[30] concerning their Pd-MOS device, and because of the fact that our analysis concerns very low partial pressures (<2000 ppm), the above assumption is reasonable. The device sensitivity to H_2, however, has also been attributed to a controversial Pd bulk effect,[33] which is incorrect according to Lundström and coworkers.[30] On the other hand, according to Fortunato *et al.*,[34] the assumption of neglecting bulk effects at high temperature (120 °C) is not valid for room-temperature operation in the case of Pd-gate MOS hydrogen detector.

From the general equation of the Langmuir isotherm adapted to our experimental conditions leading to use Eqs. (19), (20a), and (20b), we can write

$$\frac{\Theta_{is}}{1-\Theta_{is}} = \frac{\delta S_s/\delta S_{\max}}{1+(\delta S_s/\delta S_{\max})} = K(T)\sqrt{P_{H_2}}. \qquad (21)$$

Figure 4 shows the variation of $\Theta_{si}/(1-\Theta_{is})$ as a function of hydrogen concentration (or pressure) in the range of 40–2000 ppm (4–200 Pa) of hydrogen in nitrogen using a Pd film of 130 Å in thickness. This figure will be the main tool for the ensuing semiquantitative analysis based on surface and interface adsorption phenomena. Upon plotting $(\delta S_s/\delta S_{\max})/[1+(\delta S_s/\delta S_{\max})]$ vs $\sqrt{P_{H_2}}$ [see Fig. 4(a)], Eq. (21) allows $K(T)$ to be estimated from the slope of the curve (at 20 °C). We note that the curve is linear and from the slope we obtain $K(20\,^\circ\text{C}) \approx 4.7\times10^{-3}$ $(\text{Pa})^{-1/2}$. The linearity of $[\Theta_{is}/(1-\Theta_{is})]$ vs $\sqrt{P_{H_2}}$ in the range of concentrations 40–2000 ppm is consistent with Lundström's findings using his Pd-MOS device,[29,30] Langmuirian behavior at or about room temperature has already been reported by several authors. Hughes *et al.*[35] have reported Pd-thin-SiO_2-Si diodes operating at 30 °C, the H_2 response of which follows a $\sqrt{P_{H_2}}$ law up to 2000 ppm (200 Pa). In a recent publication Fortunato *et al.*[34] have also reported a Langmuirian behavior up to 2000 Pa (2×10^4 ppm) at room temperature. Equation (21) can further be rearranged to give

$$\frac{1}{\delta S_s} - \frac{1}{\delta S_{\max}} = \frac{1}{\delta S_{\max}}\,\frac{1}{K(T)\sqrt{P_{H_2}}}. \qquad (22)$$

In order to check the experimental conformity with Eq. (22), we plotted $1/\delta S_s$ vs $1/\sqrt{P_{H_2}}$ [see Fig. 4(b)]. From the slope of the linear curve of Fig. 4(b), $K(T) \approx 5.2\times10^{-3}$ $(\text{Pa})^{-1/2}$, in excellent agreement with the value determined in Fig. 4(a). Furthermore, the y-axis intercept of Fig. 4(b) gave $\delta S_{\max} \approx 1\times10^{-5}$, in good agreement with the experimental results (experimental: $\delta S_{\max} \approx 9\times10^{-6}$). Now, it is possible, in principle, to determine the temperature dependence of the constant $K(T)$, and then by plotting $\ln[K(T)]$ vs $1/T$ to obtain the value of the heat of adsorption.[30] Unfortunately, at the present time no such temperature dependent measurements are available. Using Eq. (21), it is easy to rewrite Eq. (20b) in the form of the Langmuir isotherm:

$$\delta S_s = \delta S_{\max}\Theta_{is} \approx \delta S_{\max}\left(\frac{K(T)\sqrt{P_{H_2}}}{1+K(T)\sqrt{P_{H_2}}}\right). \qquad (23)$$

Figure 3(b) (solid curve) shows Eq. (23) plotted versus P_{H_2}

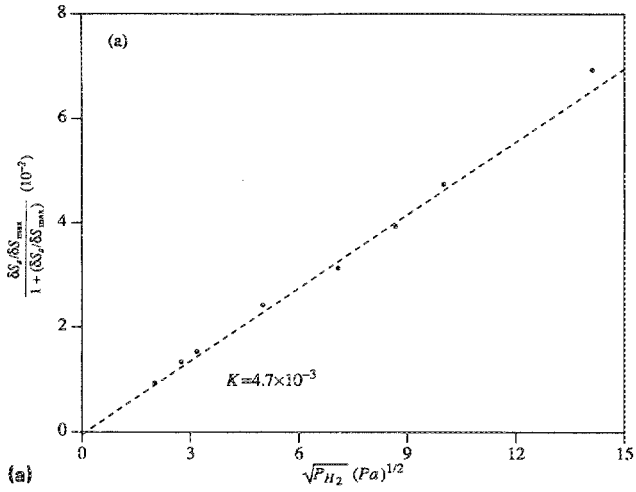

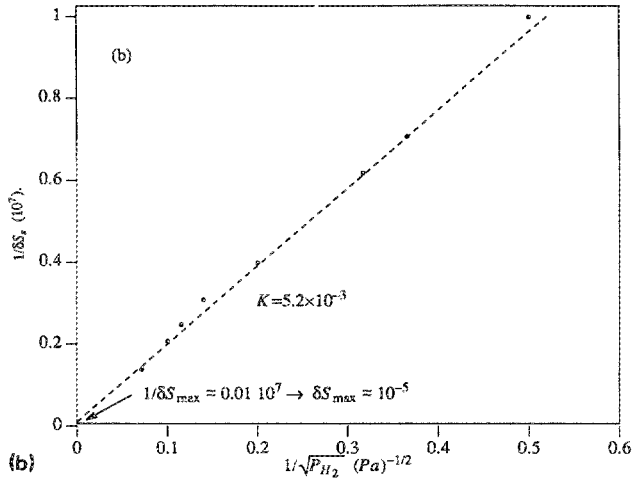

FIG. 4. (a) $(\delta S_s/\delta S_{\max})/[1+(\delta S_s/\delta S_{\max})]$ data from Fig. 3(b) plotted as a function of square root of hydrogen partial pressure, $\sqrt{P_{H_2}}$, after Eq. (21). (b) $1/\delta S_s$ plotted vs $1/\sqrt{P_{H_2}}$ after Eq. (22).

using $K(T) = 5\times10^{-3}$ $\text{Pa}^{-1/2}$. We note an agreement between the Langmuir isotherm and the experimental points especially at low pressures, where the Langmuir behavior is expected to be strictly valid. Thus the combination of the Langmuir isotherm and the photopyroelectric response gives the possibility of quantitative analysis of the signal response δS_s. We did not try to interpret any experimental results for concentrations higher than 2000 ppm (200 Pa) because the use of the Langmuir isotherm for concentrations over 2 Torr (266 Pa) is quite problematic.[36] However, it is important to note that Langmuirian behavior has also been reported by other authors up to 2000 Pa.[34] In fact, a simple adsorption mechanism is not sufficient to explain and analyze the H_2 adsorption at the interface for high pressures.[36] However, according to Lynch and Flanagan,[37] the adsorption continues after the monolayer is presumably complete. These authors have shown that, although at 37.5 °C the isotherm is almost saturated around 7 Torr ($\approx$933 Pa), at 25 °C and at the same pressure the isotherm does not show any tendancy to saturate.[37]

Equation (21) predicts that with our differential signal resolution ($\approx 10^{-8}$), the P^{2}E sensor should be sensitive to a minimum coverage $\Theta_{\min}$ at STP of approximately

$$\Theta_{\min} = \frac{\delta S_{\min}}{\delta S_{\max}} \approx \frac{10^{-8}}{9\times 10^{-6}} \approx 1.1\times 10^{-3}. \quad (24)$$

Using Eq. (21) and the minimum detectable coverage, it can be shown that the P^{2}E sensor should have the lowest pressure sensitivity $p_{\lim}$:

$$p_{\lim} = \left(\frac{\Theta_{\min}}{k_1(1-\Theta_{\min})}\right)^2 \approx 0.2 \text{ Pa}, \quad (25)$$

which corresponds to 2 ppm. This estimate is 20 times below the present experimental sensitivity limit of 40 ppm of hydrogen in nitrogen. This is probably due to the fact that the instrumental detection limit of 2 ppm is valid for measurements without any interferences from other gases, unlike the present flow-through experiments. The potential sensitivity of the P^{2}E sensor, however, to such low hydrogen partial pressures makes it a promising detection device for trace hydrogen gas analysis under STP conditions. Most importantly, the lowest (40 ppm) hydrogen concentration signal is not believed to be an absolute experimental minimum under STP. A future optimization of the setup and noise in the detection electronics is expected to improve this level of sensitivity. It ought to be mentioned that the reported sensitivity of the dc pyroelectric sensor is 1% (10 000 ppm).[17] On the other hand, it is also important to note that the P^{2}E detector is more sensitive (at room temperature) compared to some other hydrogen detectors reported by several authors such as the Pd/α-Si:H MIS Schottky barrier diode reported by Amico, Palma, and Verona.[38] The sensitivity of the above MIS detector is 100 ppm, more than two times lower that of the photopyroelectric sensor.

V. DETECTOR CHARACTERISTICS

Figure 5 shows the variation of δS as a function of time for various H_2 flow rates. We note that the flow rate does not influence δS_s much. Saturation occurs essentially at the same level, with the δS_s value being attained faster at higher flow rates, as expected. On the other hand, Fig. 6 shows that the flow rate does influence the response time of the sensor, which increases monotonically (3–10 min) with decreasing flow rate between 500 and 60 mℓ/min.

At the beginning of this effort to develop the Pd-P^{2}E detector, Pd electrodes of 985 Å in thickness were used. Unfortunately, even though the sensor was sensitive to hydrogen, its response was not reversible. After several exposures of the Pd film electrode to hydrogen, we noted that this catalyst metal began to deteriorate and peel off the PVDF film. Figures 7(a)–7(c) are three optical microscope pictures which show the Pd surface before any exposure to H_2 [Fig. 7(a)], after four to five exposures [Fig. 7(b), and after several exposures (more than ten) [Fig. 7(c)]. It is important to note that the extent of deterioration of the Pd surface was clearly visible with the naked eye. A similar phenomenon was observed by other workers, such as Armgarth and Nylander.[39] It is conceivable that this phenomenon is due to the phase change of the Pd-H_2 system. It is well known that,[26] for pressures around 2200 Pa (at 20 °C), a phase change takes place in the Pd-H_2 system. In previous work it was shown[31] that the phase change $\alpha \rightarrow \beta$ leads to an atomic lattice parameter change from 3.88 to 4.01 Å. It is probable that a phase transition from α to β may take place at low temperatures and high concentrations (1%–100%).[30] Such a change corresponds to a 10.4% increase of the Pd volume. It is thus possible that the flat portion of the curve presented in Fig. 3(a) (10%–50%) may be due to a possible phase transition. The area mismatch at the Pd-PVDF interface due to the expansion of the Pd metal is thought to cause the blisters on the Pd surface. This effect gives rise to a mechanical stress that may plastically deform the palladium film. The difference of the stress at the surface and at the interface of the Pd-PVDF is hypothesized to cause blisters. Another reason for blister formation can be found in the difference in hydrogen solubility between bulk and surface of the palladium film.

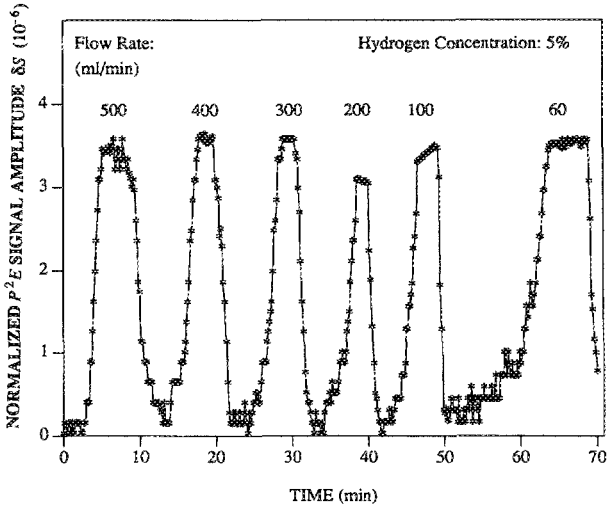

FIG. 5. Photopyroelectric signal variation as a function of time for various flow rates: 60–500 mℓ/min; $[H_2] = 5\%$ ($T = 20$ °C).

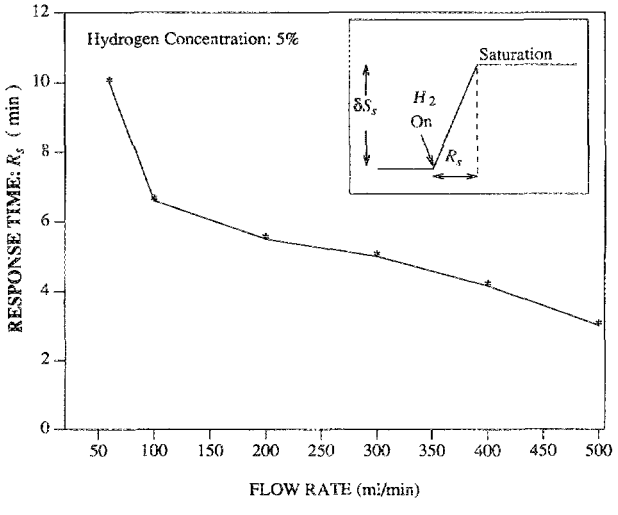

FIG. 6. Variation of response time R_s as a function of flow rate. Inset: definition of R_s.

FIG. 7. Optical microscopy of the Pd surface (985-Å thickness): (a) Before exposure to hydrogen. (b) After four to five exposures to pure hydrogen. (c) After more than ten exposures to pure hydrogen.

These ideas are also supported by (i) the fact that at very low hydrogen pressure exposures (where no phase change is expected) there were no cracks in the 985-Å Pd-PVDF system, and (ii) when the Pd thickness was decreased (285 Å) there were also no cracks even at high pressures. This is consistent with the fact[40] that with the thinner Pd films the phase change is shifted to higher pressures. At the present time more work needs to be done in identifying optimal Pd thickness on PVDF sensors. Frazier and Glosser have also shown the influence of the Pd thickness on the appearance of the phase transition.[41]

To date, we have studied the behavior of several Pd thicknesses (35–1600 Å) under various hydrogen concentrations. It is worthwhile to note that thicknesses close to 130 Å seem to be the most suitable for our photopyroelectric detector. Palladium films thicker than 1000 Å and thinner than 100 Å have been found not to be sensitive to hydrogen concentrations less than 1%. Amico, Fortunato, and Petrocco[42] described a similar phenomenon for their surface acoustic-wave sensor, but with a different thickness range (1900–7600 Å). According to these authors, among three different thicknesses of Pd coating, 1900, 3800, and 7600 Å, it is the intermediate one that presented the best response.

Using 285-Å Pd thickness as an empirical guess, the experimental results showed that the Pd-PVDF-P^2E sensor hydrogen-detection ability is completely reversible and durable. Initially, one face of the Pd-PVDF film was exposed several times to 100% H_2 (100 kPa). The experimental curves in Fig. 8(a) show an irreversible sensitivity loss with each successive introduction of hydrogen up to the fourth exposure, with well-reproducible responses upon further exposures. A similar phenomenon has been observed by Lalauze, Gillard, and Pijoalt[43] who used pure Pd substrates. A similar phenomenon concerning the pressure-concentration (P-C) isotherms as a function of the cycle of exposure to H_2 has also been reported by Quian and Northwood.[44] In fact, these authors have shown that, after five to ten absorption-desorption cycles, the hysteresis effect does not change on further absorption-desorption cycles, and this seems to be in direct relation with our own observation. According to Lalauze and co-workers,[43] however, sample treatment (exposure to H_2 and heat treatment) has a large influence on hydrogen adsorption. Our Pd-PVDF-P^2E signal saturated at a reproducible value after four or five exposures [Fig. 8(a)] without any additional treatment, unlike the work by Lalauze and co-workers,[43] who reported stabilization only after a relatively sophisticated treatment program had been followed. The stability of our sensor has been repeatedly confirmed with three different Pd-PVDF films. Figure 8(b) shows the excellent reproducibility of the signal after many exposures to pure hydrogen following the first five "break-in" exposures. This signal level has been found to be very reversible and reproducible with several Pd-PVDF films. In terms of durability, the basic signal quality shown in Fig. 8(b) lasted even after several hundred exposures and also under various hydrogen concentrations. Thus reproducibility and durability of the photopyroelectric sensor has been successfully demonstrated in this work, along with very good economic yield, considering that a 10 cm × 15 cm palla-

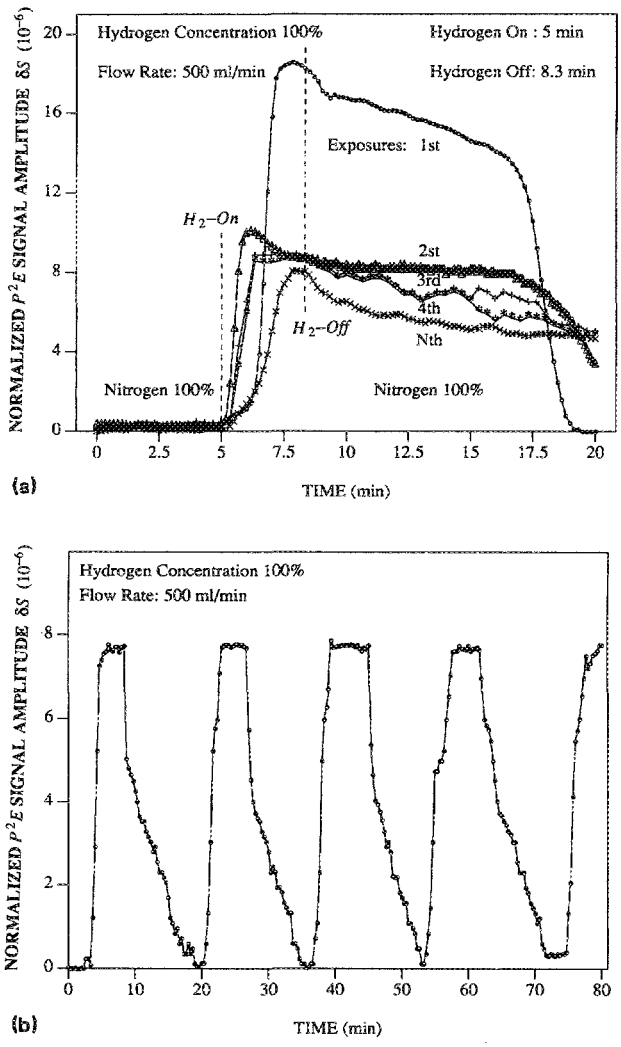

FIG. 8. Variation of the output photopyroelectric signal δS as a function of time, after several exposures to pure hydrogen: (a) With an as-received Pd-PVDF 285-Å film. (b) With a previously exposed Pd-PVDF 285-Å film.

dianized sheet of PVDF ($100) may supply 80–100 active elements which can be simply inserted in the Inficon housing to replace an old element and generate a new detector.

The direct signal dependence on heat of adsorption due to heat released to the Pd surface, following adsorption, is the dominant mechanism of the dc pyroelectric sensor, which, however, does not register in the synchronous detection mode of the ac device. Heat of adsorption will not register in the lock-in, as well as the opening and closing the valve during gas flow cycles, thus rendering the ac device immune to several pitfalls of the dc pyroelectric sensor.[17]

Some preliminary experiments at very low H_2 concentrations (20 ppm) have shown that the sensor is potentially useful at these very low concentrations. More "fine-tuned" experimentation is required to substantitate these observations and establish ultimate experimental detection limits for the P^2E sensor.

VI. CONCLUSIONS

In this paper the development of a new, sensitive, durable, and very economic Pd-PVDF-P^2E hydrogen detector has been presented. Our experimental results suggest that the investigated P^2E sensor structure can be implemented as a trace hydrogen detector, under ambient conditions or in remote locations, without the shortcomings of conventional dc pyroelectric sensors. It has been shown that, in terms of sensitivity limits, durability, and simplicity, the sensor's characteristics may be at least as good as those of other solid-state hydrogen detectors mentioned in the introduction of this paper. The room-temperature operation capability of the new P^2E sensor may also be indicative of superior durability over Pd-gate MOSFETs, the sensitivity and the response time of which at room temperature are not optimal. The main results of this study can be summarized as follows.

(1) From the point of view of the basic physics of the Pd-PVDF-P^2E detector operation, a semiquantitative phenomenological understanding has been achieved by showing that the detector response is consistent with elementary adsorption mechanisms in the Pd-H_2 system in the low H_2 partial pressure range (<200 Pa). The interpretation of our results will be more complete when the physical mechanisms generating the observed response are better understood. The sensor may further help the understanding of the Pd-H_2 interaction, as well as the dynamics of the Pd-PVDF and, more generally, the metal-polymer junction electronic behavior.

(2) It has been found that the thickness of Pd evaporated on the PVDF film plays an important role in determining sensitivity and durability. For example, it was found that thick Pd films (985 Å) lead to lower sensitivities and increased irreversibilities, probably due to the destruction of the Pd bulk by absorbed hydrogen initiating the $\alpha \rightarrow \beta$ phase change in the Pd. Thus Pd film thickness optimization is of intense interest for the optimization of the sensor characteristics (durability, reversibility, sensitivity, and speed of response). Instrumental hydrogen-detection limits were estimated to be 2 ppm.

Extensions of the present measurements for the detection of other gases may lead to an increase of the P^2E detector utility: Other environmentally important gases may be detectable, such as hydrocarbons, SO_2, HCl, NH_3, H_2S, and even radioactive gases such as tritium.

The hydrogen photopyroelectric detector could also become an excellent tool for surface science studies under UHV, especially at low temperatures where other sensors do not exhibit good performance. In fact, UHV studies will also help toward a better understanding of the operating mechanism, because of the highly controlled conditions of the ultrahigh-vacuum system.

[1] C. Christofides and A. Mandelis, J. Appl. Phys. **66**, 3986 (1989).
[2] T. Seiyama and S. Kagawa, Anal. Chem. **38**, 1069 (1966).
[3] P. J. Shaver, Appl. Phys. Lett. **11**, 255 (1967).
[4] H. Obayashi, Y. Sakurai, and T. Gejo, J. Solid State Chem. **17**, 299 (1976).
[5] K. I. Lundström, M. S. Shivaraman, and C. M. Svensson, J. Appl. Phys. **46**, 3876 (1975).
[6] K. I. Lundström, M. S. Shivaraman, and C. M. Svensson, Surf. Sci. **64**, 497 (1977).
[7] M. C. Steele and B. A. MacIver, Appl. Phys. Lett. **28**, 687 (1976).

[8]T. Yamamoto and M. Morimoto, Appl. Phys. Lett. **20**, 269 (1972).
[9]T. L. Poteat and B. Lalevic, IEEE Trans. Electron Devices **ED-29**, 123 (1982).
[10]A. D'Amico, A. Palma, and E. Verona, Appl. Phys. Lett. **41**, 3 (1982).
[11]M. A. Butler, Appl. Phys. Lett. **45**, 10 (1984).
[12]J. S. Lundsgaard, J. Malling, and M. L. S. Birchall, Solid State Ionics **7**, 53 (1982).
[13]R. V. Kumar and D. J. Fray, Sensors Actuators **15**, 185 (1988).
[14]S. Abe and T. Hosoya, in *Proceedings of the 5th World Hydrogen Energy Conference*, Toronto, Canada, 15–20 July 1984 Vol. 4, p. 1893.
[15]W. H. King, J. Environ. Sci. Technol. **4**, 1136 (1970).
[16]J. N. Zemel, B. Keramati, and C. W. Spivak, Sensors Actuators **1**, 427 (1981).
[17]J. N. Zemel, in *Solid State Chemical Sensors* edited by J. Janata and J. H. Huber (Academic, New York, 1985), Chap. 4.
[18]A. Mandelis and C. Christofides (unpublished).
[19]C. Christofides and A. Mandelis, *IEEE Ultrasonics Symposium Proceedings*, Montreal, Canada, 3–6 October 1989 (to be published).
[20]A. Mandelis and C. Christofides, *6th International Topical Meeting on Photoacoustic and Photothermal Phenomena*, Baltimore, MD, July 31–Aug. 3, 1989 (to be published).
[21]S. B. Lang, *Temperature; Its Measurement and Control* (American Institute of Physics, New York, 1962), p. 1015.
[22]S. B. Lang, *Temperature; Its Measurement and Control* (American Institute of Physics, New York, 1972), p. 1153.
[23]H. Rahnamai and J. N. Zemel, Sensors Actuators **2**, 3 (1981/82).
[24]A. Hadni, in *Infrared and Millimeter Waves* edited by K. J. Button (Academic, New York, 1980), Vol. 13, Chap 3.
[25]KYNAR Piezo Film Technical Manual (Pennwalt Corp., King of Prussia, PA, 1983).
[26]F. A. Lewis, *The Palladium/Hydrogen System* (Academic, New York, 1967), p. 94.
[27]H. J. Coufal, R. K. Grygier, D. E. Horne, and J. E. From, J. Vac. Sci. Technol. A **5**, 2875 (1987).
[28]A. Mandelis and M. M. Zver, J. Appl. Phys. **57**, 4421 (1985).
[29]K. I. Lundström, Sensors Actuators **1**, 403 (1981).
[30]I. Lundström, M. Armgarth, and L.-G. Petersson, *CRC Crit. Rev. Solid State Mater. Sci.* **15**, 201 (1989).
[31]E. A. Owen, and J. I. Jones, Proc. Phys. Soc. London **49**, 603 (1937).
[32]G. A. Somorjai, *Principles of Surface Chemistry* (Prentice-Hall, Englewood Cliffs, N.J., 1972), Chap. 5.
[33]M. C. Steele, J. W. Hile, and B. A. MacIver, J. Appl. Phys. **47**, 2357 (1986).
[34]G. Fortunato, A. Bearzotti, C. Caliendo, and A. D'Amico, Sensors Actuators **16**, 43 (1989).
[35]R. C. Hughes, W. K. Schubert, T. E. Zipperian, J. L. Rodriguez, and T. A. Plut, J. Appl. Phys. **62**, 1074 (1987).
[36]H. M. Dannetum, L.-G. Petersson, D. Söderbrery, and I. Lundström, Appl. Surf. Sci. **17**, 259 (1984).
[37]J. F. Lynch and T. B. Flanagan, J. Phys. Chem. **77**, 2628 (1973).
[38]A. D'Amico, A. Palma, and E. Verona, Appl. Phys. Lett. **3**, 31 (1982/83).
[39]M. Armgarth and C. Nylander, IEEE Electron Device Lett. **EDL-3**, 384 (1982).
[40]R. Feenstra, R. Griessen, and D. G. De Grott, J. Phys. F **16**, 1933 (1986).
[41]G. A. Frazier and R. Glosser, J. Less-Common Met. **74**, 89 (1980).
[42]A. D'Amico, G. Fortunato, and G. Petrocco, Appl. Phys. Lett. **42**, 964 (1983).
[43]R. Lalauze, R. Gillard, and C. Pijoalt, Sensors Actuators **14**, 243 (1988).
[44]S. Quian and D. O. Northwood, Int. J. Hydr. Energy **13**, 25 (1988).